The Mechanism of corrosion of MgO–CaZrO$_3$–calcium silicate materials by cement clinker

J.L. Rodríguez-Galicia [b], A.H. de Aza [a], J.C. Rendón-Angeles [b], P. Pena [a,*]

[a] *Instituto de Cerámica y Vidrio, C.S.I.C., Kelsen 5, Cantoblanco, Madrid 28049, Spain*
[b] *Centro de Investigación y de Estudios, Avanzados del IPN, Saltillo 25900, Coahuila, México*

Abstract

The chemical reactions involved in the corrosion of MgO–CaZrO$_3$–calcium silicate materials by cement clinker were studied using a hot-stage microscope up to 1600 °C. The phases formed at 1500 °C were characterized by RLOM and SEM–EDS of the crystalline phases conducted near the reaction front and on unreacted refractory area.

The general corrosion mechanism of attack on MgO–CaZrO$_3$–calcium silicate materials involves a mechanism of matter diffusion of the liquid clinker phase through the grain boundaries and pores into the refractory substrate. The liquid phases in the clinker mainly enriched in calcium, iron and aluminium are rapidly diffused and preferentially react with magnesium spinel, calcium zirconate and magnesia, which are the major constituents in the refractory substrates. The dissolution of the CaZrO$_3$ refractory phase produces the enrichment with zirconium of the liquid phase increasing its viscosity and hindering the liquid phase diffusion.
© 2006 Elsevier Ltd. All rights reserved.

Keywords: Refractories; Corrosion; MgO; CaZrO$_3$, cement clinker, microstructure

1. Introduction

Nowadays the burning zone of rotary cement kilns is exposed to alkali salts and some waste by-products such as rubber or other hazardous products of animal origin, these materials enhance the corrosion process of the kilns refractory.

Generally for a better corrosion resistance, the MgO-based materials were adopted as the main components of refractory bricks because they are hard-wearing towards the liquefied cement materials at high temperatures. MgO–MgAl$_2$O$_4$ bricks were actually used mainly in the burning zone of rotary cement kilns. These conventional materials, however, show an inadequate performance due to problems associated with corrosion resistance and their easily developing hot points.[1–3] Good alternatives for replacing the MgO–MgAl$_2$O$_4$ materials until now used, are the MgO–CaZrO$_3$–calcium silicate composite materials due to their enhanced refractoriness, high mechanical properties and excellent corrosion resistance against alkali, earth alkali oxides and basic slags.[4]

Kozuka et al.[4,5] have studied the behaviour of MgO/CaZrO$_3$ materials as a refractory materials in rotary cement kilns. The post-mortem analyses presented in these papers proved that the bricks showed superior corrosion resistance and coating adherence, but they peeled off easily in areas which underwent high mechanical stresses. Hitherto, there is only one work that describes the corrosion behaviour of MgO/CaZrO$_3$ materials with cement clinker, which was carried out by Serena et al.[6] These authors have investigated the corrosion behaviour in particular of 80 wt.% MgO–20 wt.% CaZrO$_3$ materials versus a clinker of Portland cement.

In contrast with the preliminary research works aforementioned, it was found that the use of natural raw materials constituted by major elements such as, Mg, Ca, Si and Zr is an attractive route for the production at low cost of the MgO-based high temperature structural materials. The present authors in previous works[7–9] found the mechanisms involved in the reaction sintering process for MgCa(CO$_3$)$_2$/ZrSiO$_4$ mixtures, and demonstrated that the reaction sintering is a feasible way to obtain MgO–CaZrO$_3$–calcium silicate dense composites with fine-grained microstructure. These mixtures were prepared by using mineral dolomite (MgCa(CO$_3$)$_2$) and zircon (ZrSiO$_4$)

raw materials. The composition of the mixtures prepared was tailored on the basis of the information supplied by the quaternary system MgO–CaO–ZrO$_2$–SiO$_2$[10–12] in order to obtain MgO–CaZrO$_3$–β-Ca$_2$SiO$_4$ and MgO–CaZrO$_3$–Ca$_3$Mg(SiO$_4$)$_2$ composites.

In the present work, we have explored the possibility of using the composites mentioned above that belong to the quaternary system MgO–CaO–ZrO$_2$–SiO$_2$, as refractory materials for the burning zone in rotary cement kilns.

The MgO–CaZrO$_3$–β-Ca$_2$SiO$_4$ composition is located in the solid-state compatibility plane MgO–CaZrO$_3$–Ca$_2$SiO$_4$ and lies on the connecting line zircon-dolomite Fig. 1a. The formation of the first liquid starts at 1750 °C; this temperature corresponds to the invariant point of the subsystem MgO–CaZrO$_3$–Ca$_2$SiO$_4$. From the quaternary section ZrO$_2$–SiO$_2$–CaO/MgO = 1:1 mol, it can be stated that the composition considered is located in the primary phase field of MgO[7,8] (Fig. 1b).

In accordance with Fig. 1a, the MgO–CaZrO$_3$–Ca$_3$Mg-(SiO$_4$)$_2$ composition also lies on the connecting line MgCa(CO$_3$)$_2$/ZrSiO$_4$ and is located in the solid-state compatibility plane MgO–CaZrO$_3$–Ca$_3$Mg(SiO$_4$)$_2$. This composition is also located in the primary phase field of MgO and their invariant point is low (1550 °C) (Fig. 1b). Therefore, the temperature of formation for the first liquid of compacts containing Ca$_3$Mg(SiO$_4$)$_2$ within this compatibility field, is lower than that of those formulated with β-Ca$_2$SiO$_4$.

The study described here, was focused to reveal details of the reaction behaviour at the interface of cement clinker/MgO–CaZrO$_3$–calcium silicate materials. In addition, microstructural characteristics of the reaction interface between cement clinker/MgO–CaZrO$_3$–calcium silicate materials, after corrosion treatments, were observed on specimens treated at 1500 °C for reaction intervals up to 360 min. The conditions under which different phases are formed at the interface and in the bulk of the MgO–CaZrO$_3$–calcium silicate materials, were discussed taking into account the phase equilibrium data of the systems MgO–Al$_2$O$_3$–CaO and MgO–CaO–SiO$_2$–ZrO$_2$ and compared with MgO and MgAl$_2$O$_4$ ceramic materials with similar density (≈98%) and grain size (≈4 μm).

2. Experimental

2.1. Substrate synthesis

The MgO–CaZrO$_3$–calcium silicate materials obtained in this study were prepared from a high-purity CaMg(CO$_3$)$_2$ powder (>99.9% purity, average grain size 4.9 μm, Prodomasa, Spain) and high-purity ZrSiO$_4$ powder (99.8 purity, average grain size 1.23 μm, Zircosil, Cookson Ltd.). Homogeneous dense MgO–CaZrO$_3$–calcium silicate based specimens were obtained by reaction sintering of isostatically pressed stoichiometric dolomite-zircon mixtures. The two compositions of materials were differentiated by the presence and the amount of the ternary phase β-Ca$_2$SiO$_4$ (42 vol.%) or Ca$_3$Mg(SiO$_4$)$_2$ (45 vol.%), hereafter referred to as S2 and S4, respectively. The compact density was measured by the Archimede's principle using mercury immersion. The densities thus measured for S2 and S4 specimens prepared at the temperatures (1550 and 1740 °C) reported elsewhere,[8] were 96 and 98% of the theoretical value and their average grain size measured by linear intersection method was from 1 to 6 μm. In Table 1 are summarized some typical structural properties of the materials used for the corrosion test.

A dense polycrystalline spinel (MgAl$_2$O$_4$) specimen with a grain size of few microns was produced by heating at 1600 °C a pellet isostatically pressed (200 MPa), this specimen was prepared by using high-purity spinel powders (size 7.5 μm, Baikalox, USA). Furthermore, a dense polycrystalline magnesia compact with a medium grain size of 6 ± 2 μm, was obtained by employing high purity magnesia powders (average grain size 1.4 μm, Merck, Darmstadt, Germany). The powders were isostatically pressed at 200 MPa and then sintered at 1550 °C for 2 h. Additional details of these specimens are given in Table 1.

Cylindrical plate specimens, 15 mm diameter and 4 mm thick were prepared from the four materials selected by cutting with a diamond blade. The corresponding surfaces were subsequently
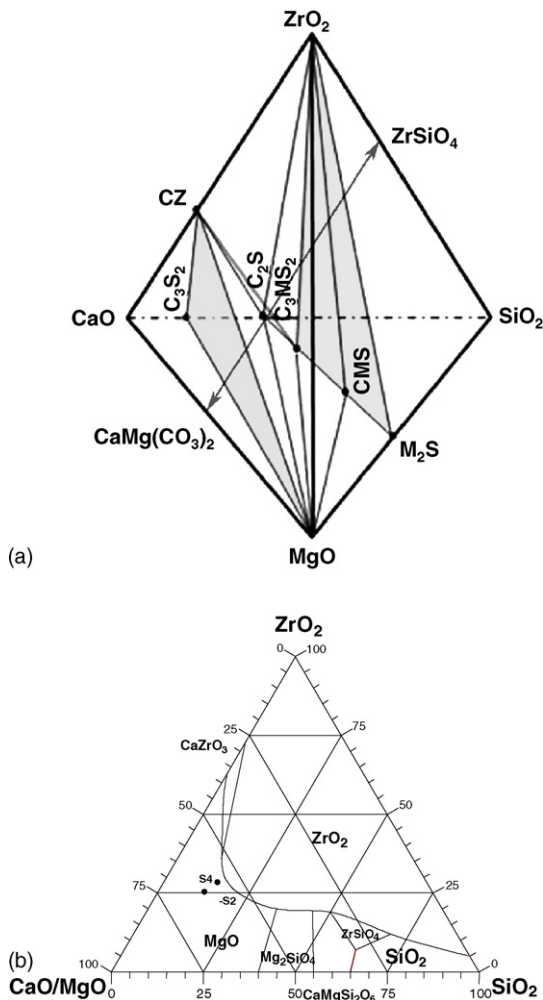

Fig. 1. Equilibrium diagram of the quaternary system MgO–CaO–ZrO$_2$–SiO$_2$: (a) solid-state compatibility relationships and (b) quaternary section ZrO$_2$–SiO$_2$–(CaO/MgO = 1 mol) section of the quaternary system showing primary phase fields of MgO, CaZrO$_3$, Ca$_2$SiO$_4$, ZrO$_2$ and the position of the studied compositions.

Table 1
Typical compositional and properties of the materials studied

	MgAl$_2$O$_4$	MgO	S2	S4
Chemical composition (wt.%)				
Al$_2$O$_3$	71.9	–	–	–
MgO	26.0	99.9	25.6	23.75
CaO	0.02	0.02	35.60	33.05
SiO$_2$	0.16	–	14.50	16.10
ZrO$_2$	–	–	24.30	27.10
K$_2$O	0.011	0.08	–	–
Physical Properties:				
Modulus of Young (GPa)	251 ± 13	270	194	181
Cold flexure strength (MPa)	200	n.d.	222	200
Toughness K_{Ic} (MPa m$^{-1/2}$)	3.0	3.0	2.1	2.6
Linear thermal expansion at 1000 °C (10^{-6} K^{-1})	8	12	12.85	9.94
Bulk Density (g/cm^3)	3.46 ± 0.03	3.58 ± 0.05	3.797 ± 0.005	3.828 ± 0.005
Crystalline phase composition (wt.%)				
MgAl$_2$O$_4$	100	–	–	–
MgO	–	100	27	20
CaZrO$_3$	–	–	31	35
Ca$_2$SiO$_4$	–	–	42	–
Ca$_3$Mg(SiO$_4$)$_2$	–	–	–	45

polished to a mirror finish using diamond paste 1 μm and then cleaned in an ultrasonic bath.

In Table 2 are summarized details of the composition for the Portland cement used in this study. The cement is composed of several minerals in which the major constituent is alite (Ca$_3$SiO$_6$). The cement raw material produced in rotary kilns, is commonly heated at 1450 °C in the burning zone. Therefore, the temperature selected to carry out the corrosion tests was 1500 °C.

2.2. Corrosion diffusion couple pair systems

In order to measure the corrosion of refractory substrates by cement clinker, the reaction test method was used. For the corrosion test, cylindrical specimens (1.5 mm diameter × 4 mm thickness) were used. These small and low compacted cylinders were placed in contact with the polished surfaces of the four ceramic materials selected in this study. Any chemical reaction between the refractory and the partially melted solid (clinker) might lead to a reactant contact, which enables the reaction to take place resulting in a matter product transport that allows the corrosion chemical reaction to proceed.

The couple diffusion systems were fired up to 1650 °C at a constant heating rate of 5 °C/min. The experiments were conducted inside a hot-stage microscope (HSM) EM 201 equipped with image analysis system and electrical furnace 1750/15 (Leica, Germany). The temperature measurements were conducted in the vicinity of the specimens with a Pt3%Rh–Pt/Pt10%Rh thermocouple, which was placed in contact with the ceramic plate used as support. The microscope projects the image of the sample through a transparent quartz window and the images were taken by a recording device. The

Table 2
Typical characteristics of Portland cement used in reaction studies

Property	Raw clinker		Clinker		
Mineralogical composition	Mineral		Mineral		wt.%
	Calcite (CaCO$_3$)		Alite (Ca$_3$SiO$_5$)		50
	Quartz (SiO$_2$)		Belite (Ca$_2$SiO$_4$)		26
	Kaolinite (Al$_2$(Si$_2$O$_5$)·(OH)$_4$)		Tricalcium aluminate (Ca$_3$Al$_2$O$_6$)		9
	Gypsum (CaSO$_4$·2H$_2$O)		Ferrite (Ca$_4$Al$_2$Fe$_2$O$_{10}$)		9
Chemical analysis (wt.%)					
Weigh loss	35.08		0.28		
Al$_2$O$_3$	3.91		5.70		
MgO	0.96		1.50		
CaO	42.96		66.06		
SiO$_2$	13.30		21.25		
Fe$_2$O$_3$	2.46		3.90		
SO$_4^{2-}$	0.11		0.85		
Density (g/cm^3)	2.7329		3.2259		

computerized image analysis system automatically records and analyzes the geometrical changes of the sample during heating. The HSM software calculates geometrical variations, such as height, width, and area of the sample; from the images and contact angle between sample and substrate.

After firing, the specimens were mounted in epoxy resin, and then cut perpendicular to the clinker–ceramic interface. The cross-section of each specimen was polished down to 1 μm roughness. Analyses of the crystalline phases were performed using reflected light optical microscopy (hereafter referred as to RLOM), and scanning electron microscopy with energy dispersive X-ray analysis (SEM/EDS) (Model DSM 950, Karl Zeiss, Thornwood, NY, USA; series, Tracor Northern, Middleton, WI, USA). Microchemical analysis of the new layer formed at the reaction interface, was carried out by SEM/EDS on samples heat treated at 1500 °C for reaction between 1 min to 2 h. Compositional line scans of CaO, Al_2O_3, Fe_2O_3, ZrO_2 and SiO_2 conducted across the clinker–ceramic interface, were made by semiquantitative analyses (SQ) using the ZAF (atomic number, absorption fluorescence) furnished software with theoretical internal standards, following the SQ program. The square area selected for microanalysis was 50 μm. More details regarding the chemical compositional analyses are given elsewhere.[13] In addition, grain size measurements, of the different crystalline phases, were carried out by using the linear interception method on representative SEM micrographs.

3. Results and discussion

3.1. Couple diffusion experiment

The reaction patterns for all the ceramic–clinker diffusion couple specimens were studied by a series of evaluations conducted on the area of the couple diffusion ceramic–clinker specimen. In each case the observation was carried out in situ during the heat treatment inside the HSM, as was explained in Section 2. From these data, the reaction temperatures at the interface on the couple ceramic–clinker were established, and because of the difference in the chemical composition of the substrates (ceramic part of the couple), it is therefore expected that different types of chemical reactions at the ceramic/clinker interface might occur.

The variation in area of the clinker specimen as a function of the temperature and substrate is shown in Fig. 2a. Photomicrographs of the shape sample evolution associated to Fig. 2a are shown in Fig. 2b, these correspond to the S2–clinker, S4–clinker, and $MgAl_2O_4$–clinker couple diffusion pairs. In this figure the typical changes in shape of three of the specimens studied for the same heating schedule can be seen. Table 3 summarizes the values of temperature at which the first and maximum shrinkage of clinker, 1350 and near 1400 °C, respectively, was observed. In the case of the sample pair $MgAl_2O_4$-clinker, an important reaction between the clinker and substrate took place at a temperature of 1450 °C (Fig. 2b). In contrast, any significant chemical reaction occurs between clinker and the other substrates (S4, S2 and MgO) even at temperatures up to 1600 °C (Fig. 2a and b).
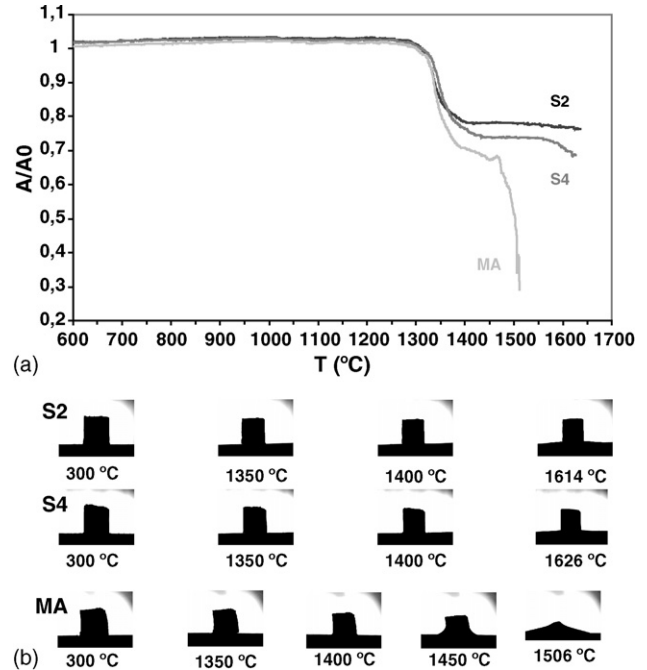

Fig. 2. (a) Variation in area of ceramic/clinker samples during hot-stage microscopy (HSM) measurements and (b) series of photomicrographs showing silhouettes corresponding to the high temperature typical behaviour pattern of the ceramic–clinker couple diffusion samples. Maximum temperature 1625 °C.

3.2. Kinetic study of the reactions at ceramic substrate/clinker interface

This study was carried out in order to make a quantitative study of the cement-clinker corrosion behaviour of different ceramic substrates with potential refractory properties. Thus, the four ceramic specimens were subjected to a chemical attack with clinker for various reaction intervals, ranging from 1 up to 120 min. The experiments were conducted inside an electric furnace following the same heat treatment conditions used in the HSM (constant heating rate of 5 °C/min and heating temperature of 1500 °C).

Fig. 3 shows the variation on thickness of the diffusion distance as a function of the reaction time, which resulted after the corrosion process between the ceramic and clinker phases. The measurements were carried out on the cross-section of polished couple diffusion samples studied by reflected light optical microscopy. As it can be seen from Fig. 3, after 1 min of reaction at 1500 °C, no chemical reaction can be detected between the MgO substrate and the clinker specimen by this technique.

Table 3
Temperatures for the fixed points in HSM (°C)

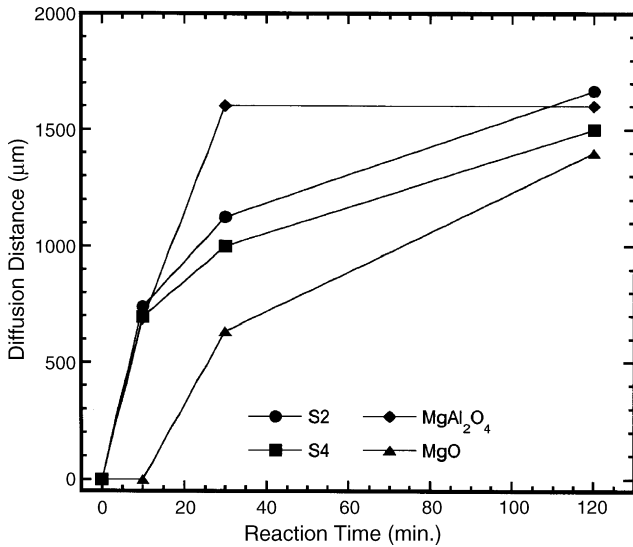| Substrate	Initial shrinkage of clinker	Maximum shrinkage of clinker	Reaction clinker/substrate	Flow
$MgAl_2O_4$	1350	1400	1450	1500
MgO	1350	≈1400	>1500	>1600
S2	1350	1400	>1600	>1600
S4	1350	1400	1600	>1600

Fig. 3. Kinetic study of the corrosion measured as the variation with time of the diffusion layer thickness at 1500 °C.

After 30 min a partial reaction was determined even by naked eye observations on couple diffusion specimens, while a characteristic clinker diffusion pattern was determined by the RLOM observations. The reaction took place mainly in the ceramic part, and the diffusion of clinker constituents towards the MgO substrate, was detected by the formation of a dense brown-coloured layer near the MgO/clinker interface. Based on our preliminary results and clinker compositional analyses (Table 2), it is suggested that, the coloration at the substrate part was mainly caused by iron diffusion. Furthermore, the formation of micro-

cracks was not detected at the interface. After the treatment for 30 min, the continuous dense and mechanically stable reaction layer resulting by the chemical interdiffusion at high temperature between clinker and ceramic substrate (MgO), had a thickness of ~600 μm (Fig. 3).

In contrast, for the $MgAl_2O_4$/clinker couple diffusion sample, the spinel was reacted with the clinker. When the experiment was conducted at a temperature (1430 °C) even lower than that used for the pair MgO/clinker (1500 °C), a complete fusion proceeded at the interface of the coupling pair $MgAl_2O_4$/clinker (Fig. 2b). The increase of the reaction time increased the penetration of the liquid phase in the spinel substrate and observations showed that the penetration of the liquid phase occurred preferentially at grain boundaries and at the residual porosity inside the substrate. Thus, in all the pair samples spinel/clinker during the course of the heating stage, it was revealed that the clinker further reacted with the ceramic substrate, in consequence the sample reached a saturation state for a reaction interval as short as 30 min (Fig. 3). The coloured layer corresponding to the reaction products is one order in magnitude higher than the reaction layer obtained on magnesia substrates, because the thickness of this layer was approximately 1600 μm.

On the other hand, for the $MgO–CaZrO_3$–calcium silicate ceramic material/clinker couple diffusion pairs, the results showed that only a partial reaction took place. The results given in Fig. 3, however, show that the reaction between clinker and $MgO–CaZrO_3$–calcium silicate materials is slightly faster than that exhibited by MgO substrate. After firing at 1500 °C for 30 min, a dense reaction layer of ~1050 μm thick was produced at the interface of both $MgO–CaZrO_3$ based substrates [S2, S4]/clinker. For the $MgO–CaZrO_3–Ca_3Mg(SiO_4)_2$/clinker
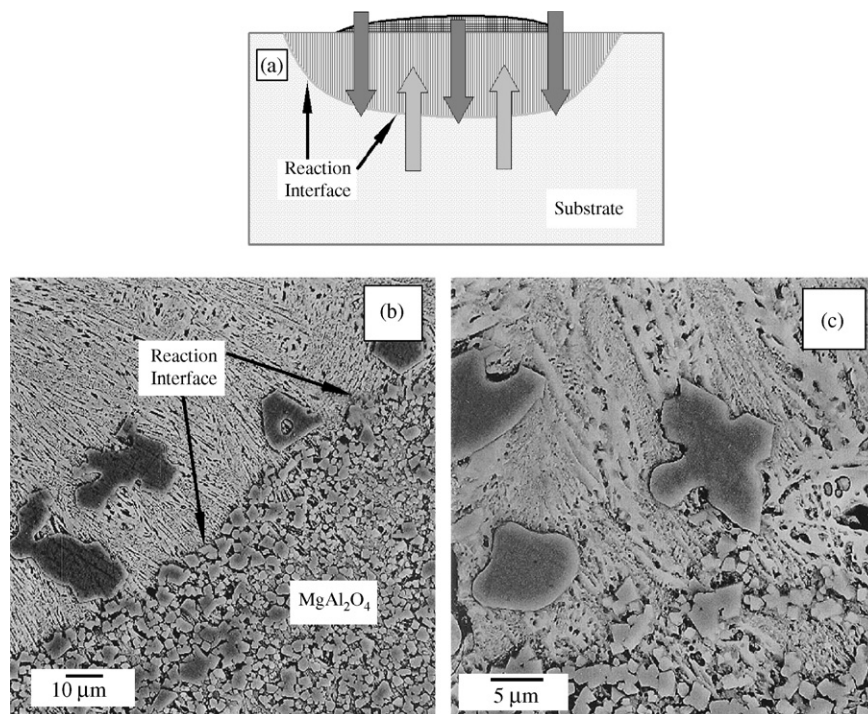

Fig. 4. (a) Sketch of the reaction mechanism; typical SEM micrographs, (b) and (c), of the cross-section for the clinker–$MgAl_2O_4$ interface of the sample fired at 1500 °C for 1 min.

specimen, bonding was also achieved over the whole interfacial area (Fig. 7), but transverse microcracking was preferentially produced along the reaction interface near the unreacted substrate part. This microcracking might occur as a consequence of the residual stresses, which may be produced during cooling stage, due to the differences in the thermal expansion coefficients of the sintered clinker and the ceramic substrate. In the case of MgO–CaZrO$_3$–Ca$_2$SiO$_4$/clinker specimen, a stronger bonding at the reaction interface of the coupling pair was achieved between the sintered clinker and substrate, in comparison with other MgO–CaZrO$_3$–calcium silicate specimens studied in this work.

The results obtained in the present study, bear clear evidence regarding the corrosion resistance of refractory substrates with cement clinker. It is proposed that the corrosion resistance of the Mg-based ceramic increases in the following sequence:

MgAl$_2$O$_4$

    < MgO–CaZrO$_4$–calcium silicate based materials < MgO

3.3. Microstructural and microchemistry studies of reaction interface of couple diffusion pairs

3.3.1. MgAl$_2$O$_4$ substrate

Fig. 4a shows a schematic representation of the reaction occurring at the interface (clinker–MgAl$_2$O$_4$) at high temperature (1500 °C) for 1 min. It is worth noting that the interface inside the MgAl$_2$O$_4$ substrate is well-defined, because it is different in composition and microstructure as preliminary naked eye observations had revealed. Furthermore, details of the microstructure and composition of the phases revealed that the reaction interface is located inside the ceramic substrate (Fig. 4b and c). Microstructures of Fig. 4 showed the presence of a devitrified glassy phase, liquid at the experiment temperature, which was produced by the chemical reaction between the clinker and MgAl$_2$O$_4$ (Fig. 4b). Some primary spinel crystals that precipitated in the glassy phase/substrate interface are also visible (Fig. 4c). The mentioned liquid phase diffused through the spinel grain boundaries and pores forming a tiny layer surrounding the spinel grains. This liquid layer is likely to dissolve the spinel crystals.

3.3.2. MgO substrate

An SEM micrograph of MgO specimen treated at 1500 °C for 1 min is shown in Fig. 5. In this micrograph the formation of a reaction layer between substrate and partially fused clinker was revealed (Fig. 5a). Energy dispersive X-ray point analyses showed that the partially melted clinker contains primary Ca$_3$Al$_2$O$_6$ crystals and a white glassy phase with a composition of 50 wt.% CaO, 24 wt.% Al$_2$O$_3$, 19 wt.% Fe$_2$O$_3$, 4 wt.% SiO$_2$ and 3 wt.% of MgO. This glassy phase was produced by melting the secondary crystalline phases, Ca$_2$SiO$_4$ and Ca$_4$Al$_2$Fe$_2$O$_{10}$, of the clinker. The micrograph of the clinker–magnesia interface shows the presence of a thin liquid phase layer at the MgO grain boundaries (Fig. 5b). This liquid phase is mainly constituted by Fe, Al, Mg, Si and Ca. The concentration profile determined
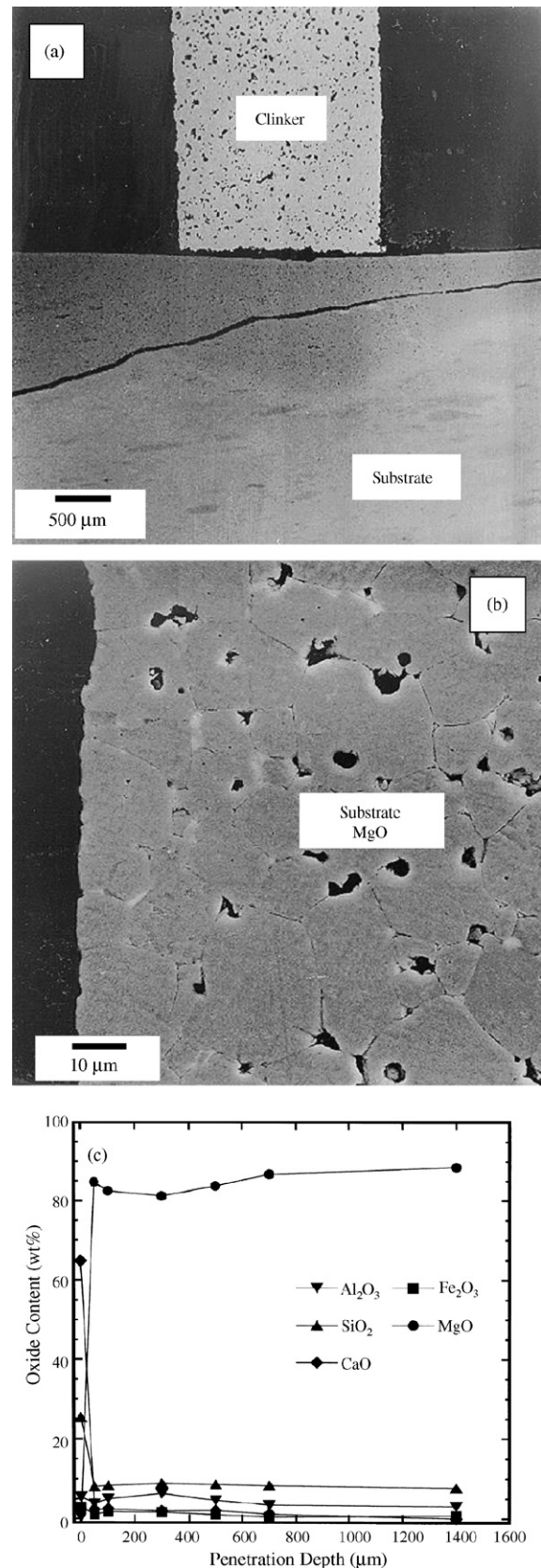

Fig. 5. (a) General SEM observations of the cross-section of the clinker–MgO sample fired at 1500 °C for 1 min; (b) micrograph of the interface clinker-spinel showing the bright triple point phases; and (c) compositional profiles of reacted zone – reaction product – slag.

along the boundary clinker/substrate indicates that the value of CaO/SiO_2 ratio was increased at the inner MgO interface. Iron and silica diffusion was observed even at a distance of 1400 μm (Fig. 5c). The presence of liquid phases in the grain boundaries produced a marked growth of magnesia grains, because the size of the MgO grains at the unreacted zone measured at a distance of 1400 μm was smaller (6 ± 2 μm) than that at the magnesia/clinker interface (13.7 ± 2 μm).

3.3.3. MgO–CaZrO₃–calcium silicate based substrates

Fig. 6 shows typical SEM micrographs taken at the cross-section of the MgO–CaZrO₃–β-Ca₂SiO₄/clinker specimen fired at 1500 °C for 1 min. In this micrograph the formation of several layers between substrate and clinker occurred, as can be observed in Fig. 6a. The microstructure near to the reaction boundary clinker/substrate exhibits the presence of the partially melted clinker Fig. 6b, which is constituted by primary $Ca_3Al_2O_6$ crystals and a glassy phase. The composition of the glassy phase was about 50 wt.% CaO, 24 wt.% Al_2O_3, 19 wt.% Fe_2O_3, 4 wt.% SiO_2 and 3 wt.% of MgO. Furthermore, a marked

formation of dark semi-spherical MgO grains which align parallel to the reaction interphase occurred near the reaction front. This MgO grain layer has a thickness of about 20 μm Fig. 6b. The main constituents determined in this thin layer were identified as MgO and liquid. In addition, SEM micrographs of Fig. 6a showed a broad zone, ∼500 μm thick, constituted according to MEB-EDS microanalyses and XRD analyses by the following crystalline phases: continuous and twinned grey grains of β-Ca_2SiO_4, 4 μm size; dark periclase (MgO) grains with a size of 2 μm and white semi-spherical 2 μm size grains of $CaZrO_3$ located at the grain boundaries or triple points (Fig. 6c). The analysis of the liquid phase, isolated glassy phase (GF) islands, arrows in Fig. 6c, showed that it contained Fe, Al, Mg, Si, Ca and a small amount of Zr. This glassy phase was detected in the MgO/CaZrO₃ boundaries or triple junctions, but not at $CaSiO_4$ grain boundaries.

Fig. 6d shows the compositional profile of S2–clinker specimen determined by EDS at the area where the reaction took place. The content of different elements, as oxides, was represented as a function of the penetration distance from the
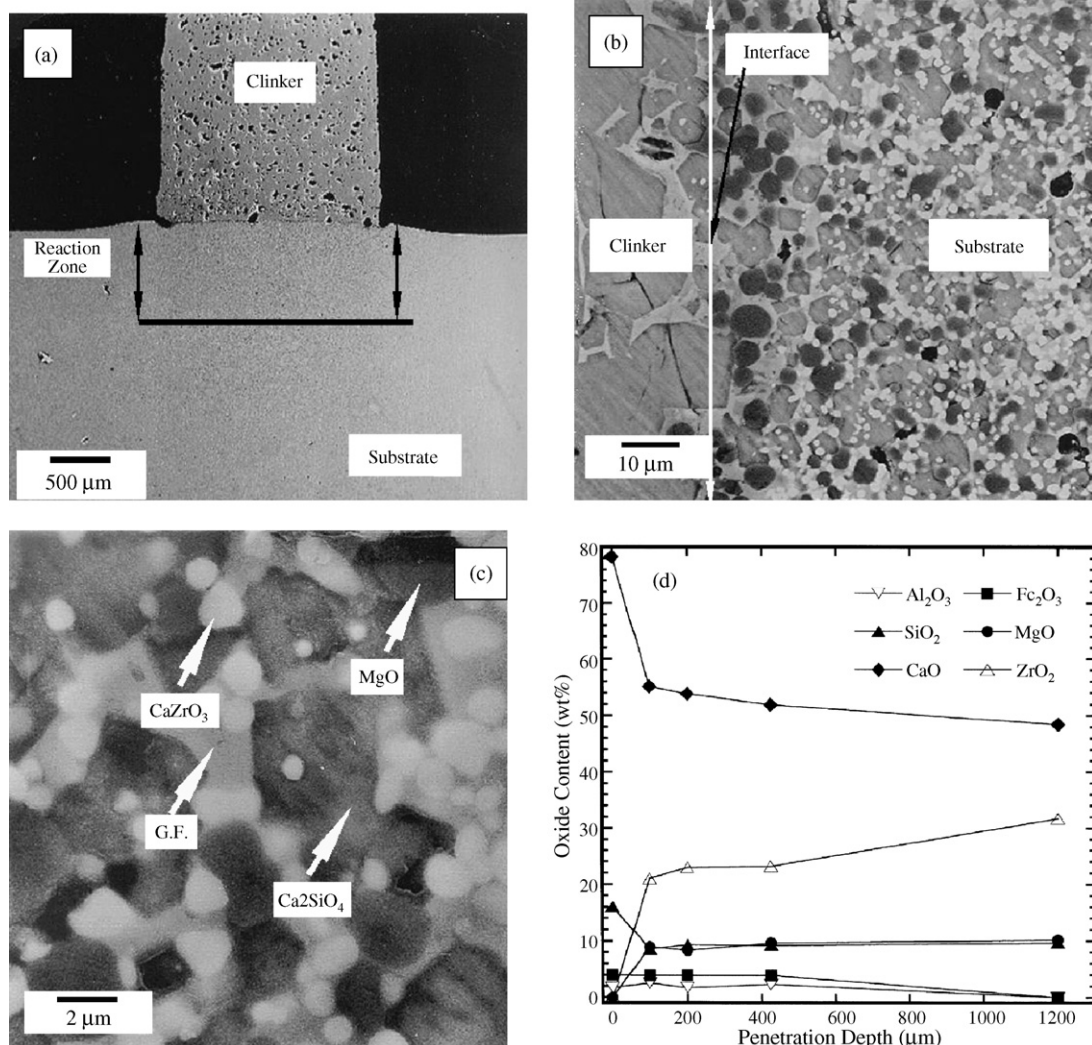

Fig. 6. (a) General SEM view of the cross-section of the clinker/S2 sample fired at 1500 °C for 1 min; (b) micrograph of the interface clinker-S2 showing periclase grains; (c) details of reacted zone showing the liquid phase detected in the CaZrO₃ grain boundaries; (d) compositional profiles of reacted zone.
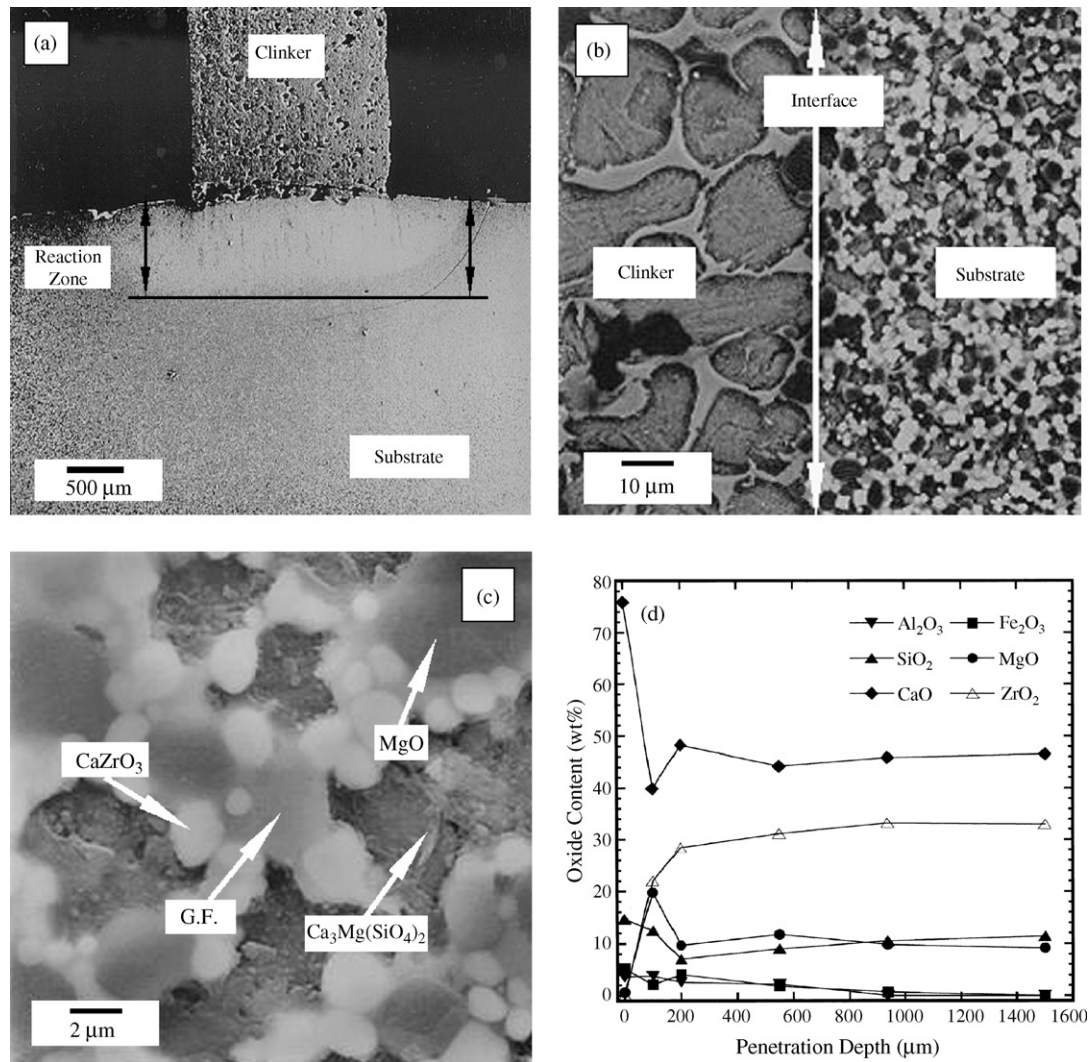
Fig. 7. (a) General SEM view of the cross-section of the clinker/S4 sample fired at 1500 °C for 1 min; (b) micrograph of the interface clinker-S4; (c) details of reacted zone showing the liquid phase detected in the $CaZrO_3$ grain boundaries; (d) compositional profiles of reacted zone.

clinker/substrate interface. The diffusion of the clinker liquid phase proceeded trough the grain boundaries, as it was suggested by the presence of Fe and Al traces that can be observed until 400 μm depth. At a distance 1200 μm from the reaction interphase, the microanalysis showed no further compositional changes in comparison with the nominal amount of the crystalline phases in the raw ceramic substrate. The microstructure is in good agreement with the chemical compositional measurements, because at this area the raw microstructure of the ceramic substrate was observed after the high temperature corrosion test.

Fig. 7a shows a macroscopic SEM view of the cross-section of coupling pair $MgO–CaZrO_3–Ca_3Mg(SiO_4)_2$/clinker sample, fired at 1500 °C for 1 min. Further, microstructural details at the reaction interphase are shown in Fig. 7b. It was found that in this particular case, the microstructure of clinker was composed by a crystalline Ca_3SiO_5, primary phase of clinker and a white glassy phase containing Ca, Al, Fe, Si, and Mg as the dominant chemical constituents. This glassy phase was homogeneously

distributed around Ca_3SiO_5 grains (see Fig. 7c). Fig. 7d shows a compositional profile for the S4-clinker specimen. The presence of Fe and Al, which act as tracing elements for the liquid clinker diffusion, was only determined up to a penetration distance of 600 μm. Beyond this distance, no further migration of the liquid phase was detected in the ceramic substrate, as was determined by both compositional and microstructural analyses.

In Fig. 7a–c the formation of a $MgO–CaZrO_3–Ca_3Mg$-$(SiO_4)_2$ liquid layer between S4 substrate and clinker was observed. According to SEM–EDS microanalyses and XRD analyses, the crystalline phases identified in this zone of the sample were as follows: corroded light grey areas (4 μm size) of merwinite crystals ($Ca_3Mg(SiO_4)_2$) and a liquid phase, formed by partial dissolution of merwinite by the diffusing liquid phase; dark rounded periclase grains with a grain size of 2 μm, and white rounded $CaZrO_3$ grains of 2 μm. In the liquid phases analysed Fe, Al, Mg, Si, Ca and small amounts of Zr were detected. Moreover, small amounts of glassy phase were detected in $CaZrO_3$ and magnesia/$CaZrO_3$ boundaries or triple junctions.

One point that deserves emphasize is that when S4 sample was subjected to long time experiments (120 min) it exhibited a dusting process. This phenomenon did not allow completing the corrosion ceramic–clinker interface microscopic study because the interface falls apart during the diamond polishing stage.

4. Corrosion mechanism

In general, the corrosion study conducted on various ceramic substrates, indicated that at the initial stages of the corrosion process, interdiffusion and chemical reaction processes between various components of the liquid phase formed in the clinker and the refractory materials (substrates) markedly occurred. Therefore, the results obtained were discussed in terms of the phases predicted in the respective equilibrium diagrams.[14,15]

In all samples the corrosion took place by diffusion of the clinker liquid phase through grain boundaries and the residual porosity. This inference was also supported by all compositional profiles where the elements such as Al, Ca, Si and Fe had marked diffusion patterns. In accordance with the chemical composition of the liquid phase formed by fusing the clinker, the constituents are 50 wt.% CaO, 24 wt.% Al_2O_3, 19 wt.% Fe_2O_3, 4 wt.% SiO_2 and 3 wt.% of MgO. The chemical composition of the liquid phase will be similar to that of the quaternary invariant point corresponding to the Portland cement clinker,[16] Ca_2SiO_4–Ca_3SiO_5–$Ca_3Al_2O_6$–$Ca_4Al_2Fe_2O_{10}$ (peritectic, 1338 °C). Therefore, as a first approach we suggested that this composition is nearly similar to that for the ternary invariant point Ca_3SiO_5–Ca_2SiO_4–$Ca_3Al_2O_6$ (peritectic at 60 wt.% CaO, 30 wt.% Al_2O_3, 10 wt.% SiO_2 and ∼1455 °C) of the ternary system CaO–SiO_2–Al_2O_3.[17]

4.1. $MgAl_2O_4$ substrate

In this particular case, it was found that the spinel substrate reacts with clinker at 1450 °C forming a liquid phase. This liquid phase wetted the spinel grains and diffused inside the specimen by a grain boundary mechanism, as can be seen in Fig. 4, filling open pores and triple points. The major constituents of the cement clinker liquid phase[17] are Ca, Al, Si, and Fe oxides, and minor Mg. As a first approach, it is suggested that the most corrosive component in the liquid is calcium oxide. We explain this inference by analysing the reactions predicted in the ternary system Al_2O_3–CaO–MgO,[18] in order to interpret the corrosion behaviour of the spinel substrate with clinker.

In Fig. 8 is shown an isothermal section corresponding to the Al_2O_3–CaO–MgO system at 1500 °C. In this system the composition of clinker glassy phase, is almost $Ca_3Al_2O_6$. Therefore, the working compositions for the liquid clinker corrosion may be represented by a line going from the $Ca_3Al_2O_6$ up to the $MgAl_2O_4$. Hence, the liquid must gradually dissolve the spinel substrate, and a change on composition of the liquid phase is likely to occur along this line. In addition, based on our observations, the primary spinel phase is in equilibrium with the calcium aluminate liquid phase, L_B, at 1500 °C. The dissolution of spinel by this glassy phase continues until it reaches the equilibrium and at this point about 30% of liquid, L_R, might coexist with
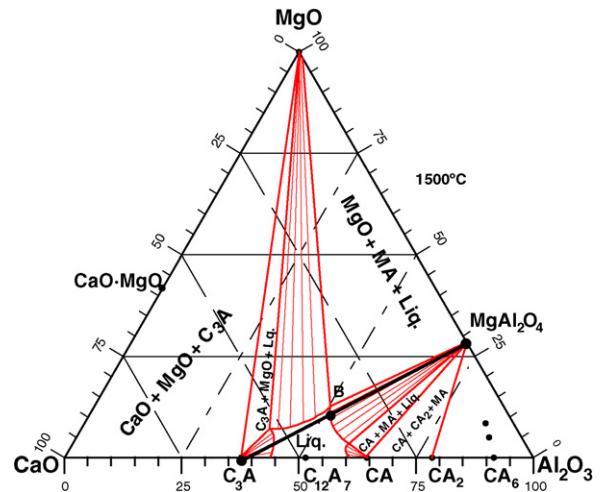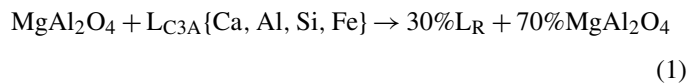

Fig. 8. Isothermal section of Al_2O_3–CaO–MgO ternary diagram at 1500 °C.

$MgAl_2O_4$ as indicated by the following equation:

$$MgAl_2O_4 + L_{C3A}\{Ca, Al, Si, Fe\} \rightarrow 30\%L_R + 70\%MgAl_2O_4$$

(1)

4.2. MgO substrate

In contrast, in periclase substrates, at temperatures higher than 1500 °C, some extent of reaction with clinker is observed. Likewise in the clinker–$MgAl_2O_4$ substrates, the reaction interface clinker–MgO may be interpreted from the 1500 °C isothermal section of MgO–CaO–Al_2O_3 ternary phase diagram Fig. 8. In this case, the working compositions are represented by the compatibility line going from $Ca_3Al_2O_6$ to MgO, therefore no liquid phase formation would occur at 1500 °C.

The presence of SiO_2 in the clinker liquid phase, however, decreases the temperature for the first liquid formation[18–20] up to approximately 1380 °C, so the discussion stated on the basis of the MgO–CaO–Al_2O_3–SiO_2 phase diagram. The phases identified at the interface, liquid + MgO + Ca_3SiO_5, are those predicted from the MgO-rich region in the MgO–CaO–Al_2O_3–SiO_2 quaternary phase equilibrium diagram.[21,22] The eutectic in the quaternary subsystem MgO–Ca_3SiO_5–Ca_2SiO_4–$Ca_3Al_2O_5$ takes place at 1380 °C, but the amount of liquid phase might be very small due to the big size of periclase primary phase field. So, the presence of small amounts of liquid phase at periclase grain boundaries might be explained in terms of a diffusion mechanism of the quaternary liquid phase.[20] This liquid phase, at high temperatures, partially dissolves primary MgO grains enhancing subsequently their grain growth, and also achieves the substrate densification in the reaction zone by a liquid reaction sintering process.

The presence of small amounts of liquid phases, rich in Ca^{2+}, Al^{3+}, Si^{4+}, and $Fe^{2+,3+}$, which penetrate through the periclase grain boundaries, is explained in terms of a diffusion mechanism of the clinker liquid phase.

4.3. MgO−CaZrO₃−calcium silicate substrates

The two derived MgO−CaZrO₃−calcium silicate substrates composite materials have similar microstructural parameters (Table 3), grain size and shape, the main difference between them is the composition of the ternary phase, which was in similar amounts in both composites.

In the two MgO−CaZrO₃−calcium silicate substrates/clinker interfaces the presence of a thick layer formed by MgO grains was detected. The enrichment in MgO at the clinker–ceramic interface can be explained in terms of the quaternary system MgO−CaO−ZrO₂−SiO₂ (Fig. 1b). Based on this diagram, it is suggested that at clinker/substrate interface the first liquid formation for the two compositions considered, S2 and S4, occurs at the invariant point temperature for the subsystems MgO−CaZrO₃−Ca₂SiO₄ (1750 °C) and MgO−CaZrO₃−Ca₃Mg(SiO₄)₂ (1550 °C), respectively. From this diagram, it can be seen also that the two compositions are located in the MgO primary phase field. Therefore, the last phase that is dissolved in the diffusing clinker Ca−Si rich liquid phase must be MgO. The presence of Al₂O₃ and Fe₂O₃, however, decreases the temperature for the first liquid formation[18–20] up to approximately 1200 °C, so the discussion stated on the basis of the MgO−CaO−ZrO₂−SiO₂ phase diagram allows to interpret correctly the corrosion behaviour of the samples, but the temperatures of first liquid formation must be significantly lower.

At the test temperature, 1500 °C, in the MgO−CaZrO₃− calcium silicate substrates the liquid phase of clinker containing Si, Ca, Al, Mg and Fe also diffuses through the grain boundaries. This liquid phase coming from the clinker reacts by different pathways: (a) the Ca₃Mg(SiO₄)₂ is dissolved by the liquid forming a CaO-rich liquid phase which promoted precipitation and growing of the stable phase β-Ca₂SiO₂; (b) the CaZrO₃ grains are partially dissolved causing an enrichment in Zr⁴⁺ of the liquid phase; (c) the periclase (MgO) grains slightly dissolve in the liquid; and (d) the diffusing liquid phase partially dissolves Ca₂SiO₄ increasing the amount of liquid at the reaction zone.

One point that deserves emphasis is one related to the CaZrO₃ dissolution, because this phase increases Zr⁴⁺ in the liquid. The presence of Zr⁴⁺ in the liquid phase increases its viscosity and hinders the liquid phase diffusion resulting in a high corrosion resistance of these materials. In addition, both MgO−CaZrO₃−calcium silicate materials, differentiated by the crystalline constituents β-Ca₂SiO₄ or Ca₃Mg(SiO₄)₂, in accordance with the stoichiometry of the starting mixture and the related reactions at clinker/substrate interfaces, it is suggested that those phenomena strongly depend on the calcium silicate phase constitution.

The microscopic study of corrosion interface could not be conducted due to the dusting process during post-mortem analyses for long-term experiments (120 min) in MgO−CaZrO₃−Ca₃Mg(SiO₄)₂ samples. The disintegration of the reaction interface is attributed to the polymorphic, martensitic type crystalline transformation of β-Ca₂SiO₄ to γ-Ca₂SiO₄ during the cooling stage. This particular crystalline transfor-

mation occurs at 675 °C and the volume change associated is approximately of 12%. The change in volume affects markedly grains with sizes higher than 5 μm.[23] This effect may be explained in terms of a grain growth, which might occur if the corrosion goes through a dissolution of Ca₃Mg(SiO₄)₂ and a precipitation of the high calcium content phase β-Ca₂SiO₄. Furthermore, the mentioned dusting phenomenon was not observed in MgO−CaZrO₃−β-Ca₂SiO₄ sample (S2). This is attributed to the size of β-Ca₂SiO₄ grains, which remain small even after long time corrosion experiments. It is therefore suggested that this reaction occurs in the presence of significant amounts of glassy phase.

From the results obtained in the present post-mortem study it is clear that the corrosion behaviour of the substrates by cement clinker can be classified as:

MgO very good, S4 and S2 good and MgAl₂O₄ bad.

In summary, at the initial step of the corrosion process, the liquid phase of clinker penetrates inside the substrates through open porosity and grain boundaries. This liquid phase produces a significant reactive sintering process in porous substrates (MgO, MgAl₂O₄) while a partial dissolution of Ca₃Mg(SiO₄)₂, CaZrO₃ and MgO occurs. The marked dissolution of CaZrO₃ grains promoted the enrichment of the liquid phase with Zr⁴⁺, which increased its viscosity. The phases identified in the interface Ca₃SiO₃ + MgO + liquid are as expected to form from the CaO−SiO₂−MgO major oxides at this point of the diffusion coupling pair samples. Finally, in MgO−CaZrO₃ substrates the presence of secondary phases is also beneficial to prevent the exaggerated grain growth by pinning.

5. Conclusions

The mechanism of corrosion in MgO−CaZrO₃−calcium silicate based materials by clinker has been clarified in situ by hot-stage microscopy up to 1600 °C and scanning electron microscopy with energy dispersive microanalyses on corroded and quenched samples. From the post-mortem microstructural study, it has been found that the corrosion occurs by a diffusion mechanism of the clinker liquid phase through the grain boundaries and open pores in all the studied refractory substrate materials. This liquid phase partially dissolves the MgAl₂O₄, Ca₃Mg(SiO₄)₂, CaZrO₃ and MgO phases.

In CaZrO₃ containing materials, the reaction with the clinker liquid phase allows the formation of a zirconium containing silicate liquid boundary layer, which is adjacent to the calcium zirconate grains near to the clinker–substrate interface. The presence of Zr⁴⁺ in this liquid phase increases its viscosity and hinders the liquid phase diffusion enhancing the corrosion resistance of these materials.

In contrast, the aluminum magnesium spinel material is markedly dissolved, up to 30%, explaining the behaviour of spinel magnesia refractories, which are currently used in the clinkering zone of the rotary cement kilns. It is hence concluded that the good corrosion resistance of the derived MgO−CaZrO₃−calcium silicate materials makes them an attractive material to produce binder fine filler for magnesia chrome-

free refractory bricks, which are used at the burning zone of rotary cement kilns.

Acknowledgements

References

1. Bartha, P. and Klischat, H. J., Present state of the refractory lining for cement kilns. *CN-Refractories*, 1999, **6**(3), 31–38.
2. Komatsu, H., Arai, M. and Ukawa, S., Current and future status of chrome-free bricks for rotary cement kilns. *Taikabutsu Overseas*, 1999, **19**(4), 3–9.
3. Bartha, P. and Klischat, H. J., Classification of magnesia bricks in rotary cement kilns according to specification and service-ability. *ZKG Intern.*, 1994, **47**(10), E277–E280.
4. Kajita, Y., Honda, T., Kozuka, H., Tsuchiya, Y., Sakakibar, K. and Tanemura, F., *Taikabutsu*, 1991, **43**(2), 89–90.
5. Kozuka, H., Kaita, Y., Tuchiya, Y., Honda, T. and Ohta, S., New kind of chrome-free (MgO—CaO—ZrO$_2$) bricks for burning zone of rotary cement kiln. *Unitecr. 93, Sao Paulo, Brasil*, 1993, 1027–1037.
6. Serena, S., Sainz, M. A. and Caballero, A., Corrosion behaviour of MgO/CaZrO$_3$ refractory matrix by clinker. *J. Eur. Ceram. Soc.*, 2004, **24**, 2399–2406.
7. Rodríguez, J. L., Rodríguez, M. A., De Aza, S. and Pena, P., Reaction sintering of zircon-dolomite mixtures. *J. Eur. Ceram. Soc.*, 2001, **21**, 343–354.
8. Rodríguez, J. L., Baudin, C. and Pena, P., Processing and mechanical characterization of periclase-calcium zirconate based materials obtained by reaction sintering of zircon-dolomite mixtures. *J. Eur. Ceram. Soc.*, 2004, **24**, 669–679.
9. De Aza, A. H., Turrillas, X., Rodríguez, J. L. and Pena, P., Estudio del proceso de sinterización reactiva en sistemas con dolomita mediante termodifractometria de neutrones. *Bol. Soc. Esp. de Ceram. V.*, 2004, **43**(1), 12–15.
10. De Aza, S., Richmond, C. and White, J., Compatibility relationships of periclase in the system CaO—MgO—ZrO$_2$—SiO$_2$. *Trans. J. Br. Ceram. Soc.*, 1974, **73**(4), 109–116.
11. Serena, S., Sainz, M. A. and Caballero, A., Experimental determination and thermodynamic calculation of the ZrO$_2$—CaO—MgO system at 1600°, 1700° and 1750 °C. *J. Am. Ceram. Soc.*, 2004, **87**(12), 2268–2274.
12. Rodríguez, J. L., Ph.D. thesis, Universidad Autónoma de Madrid, 2001 (in Spanish).
13. McCarthy, J. J. and Schamber, F. H., Least squares fit with digital filter in a status report to the National Bureau Standards, Special Publication 604. In *Proceedings of workshop on April 1979*. National Bureau Standards, Gaithersburg, MD, 1979, pp. 273–296.
14. Phase Diagrams for Ceramists, ed. E. M. Levin, C. R. Robbins, H. F. McMurdie. The American Ceramic Society. Inc., 1964, pp. 219–220.
15. De Aza, A. H., Pena, P. and De Aza, S., Ternary system Al$_2$O$_3$—MgO—CaO: I, primary phase field of crystallization of spinel in the subsystem: MgAl$_2$O$_4$—CaAl$_4$O$_7$—CaO—MgO. *J. Am. Ceram. Soc.*, 1999, **82**(8), 2193–2203.
16. De la Torre, A., Aranda, M. A. G., De Aza, A. H., Pena, P. and De Aza, S., Belite Portland Cements. Synthesis and mineralogical analysis. *Bol. Soc. Esp. Ceram. V.*, 2005, **44**(3), 185–191.
17. Swayze, M. A., A report on studies of 1. The ternary system CaO–C$_5$A$_3$–C$_2$F. 2. The quaternary system CaO–C$_5$A$_3$–C$_2$F–C$_2$S. 3. The quaternary system as modified by 5-percent magnesia. *Am. J. Sci.*, 1946, **244**(1), 1–30.
18. De Aza, A. H., Iglesias, E., Pena, P. and de Aza, S., The ternary system Al$_2$O$_3$—MgO—CaO. Part II. Phase relationships in the subsystem Al$_2$O$_3$—MgAl$_2$O$_4$—CaAl$_4$O$_7$. *J. Am. Ceram. Soc.*, 2000, **83**(4), 919–927.
19. Fabrichnaya, O. B. and Nerád, I., Thermodynamic properties of liquid phase in the CaO·SiO$_2$–CaO·Al$_2$O$_3$·2SiO$_2$–2CaO·Al$_2$O$_3$·SiO$_2$ system. *J. Eur. Ceram. Soc.*, 2000, **20**(4), 505–515.
20. Jak, E., Thermodynamic modelling of the system Al$_2$O$_3$—SiO$_2$—CaO—FeO—Fe$_2$O$_3$ to predict the flux requirements for coal ash slags. *Fuel Energy Abstr.*, 1998, **39**(3), 231.
21. Bigger, G. M. and O'Hara, M. J., Retrograde solubility of periclase, forsterite and dicalcium silicate. *J. Am. Ceram. Soc.*, 1979, **53**(10), 538–540.
22. Koch, V. K., Trömel, G. and Heinz, G., Das Zustandsdiagramm Al$_2$O$_3$—CaO—MgO—SiO$_2$ in polythermischer Darstellung. *Tonind.-Ztg. Keram. Rundsch.*, 1975, **99**(3), 57.
23. Burggraaf, A. J., Science of ceramics. In *The Nederlandse Keramishe Vereninging, Vol 9*, ed. K. J. de Vries, 1977, p. 292.